

ASK: Adaptive Self-improving Knowledge Framework for Audio Text Retrieval

Siyuan Fu^{1*}Xuchen Guo^{1*}Mingjun Liu^{1*}Hongxiang Li²Boyin Tan³Gongxi Zhu⁵Xianwei Zhuang⁴Jinghan Ru⁴Yuxin Xie^{4†}Yuguo Yin⁴¹University of Electronic Science and Technology of China²Hong Kong University of Science and Technology³Mohamed Bin Zayed University of Artificial Intelligence⁴Peking University⁵Tsinghua University

siyuanfu05@gmail.com, yuxinxie2001@gmail.com

ABSTRACT

The dominant paradigm for Audio-Text Retrieval (ATR) relies on dual-encoder architectures optimized via mini-batch contrastive learning. However, restricting optimization to local in-batch samples creates a fundamental limitation we term the Gradient Locality Bottleneck (GLB), which prevents the resolution of acoustic ambiguities and hinders the learning of rare long-tail concepts. While external knowledge injection can break this bottleneck, it often triggers a problem called Representation-Drift Mismatch (RDM), where a static knowledge base becomes misaligned with evolving encoders, degrading guidance into noise. To address these intertwined challenges, we propose the **Adaptive Self-improving Knowledge (ASK)** framework. ASK breaks the GLB via multi-grained knowledge injection and mitigates RDM through a dynamic refinement strategy that synchronizes the knowledge base with the model. Additionally, an adaptive reliability weighting scheme is employed to filter retrieval noise based on cross-modal consistency. Extensive experiments across multiple benchmarks demonstrate that ASK consistently achieves new state-of-the-art performance across various backbones.

1 Introduction

Audio-Text Retrieval (ATR) aims to establish a shared embedding space where acoustically and semantically corresponding audio and text pairs are aligned [Mei et al., 2022, Yan et al., 2024]. The dominant paradigm currently relies on dual-encoder architectures optimized via contrastive learning objectives, such as the NT-Xent loss [Chen et al., 2020]. As illustrated in Figure 1 (left), this approach refines representations by maximizing the similarity between matched pairs while contrasting them against other samples within the same mini-batch. While effective, this in-batch mechanism implicitly restricts the optimization landscape to the local context.

The limitations of such batch-constrained optimization have been extensively discussed in broader representation learning literature, particularly regarding the necessity of large negative pools [He et al., 2020, Xiong et al.]. Building on these observations, we define this phenomenon in the context of ATR as the Gradient Locality Bottleneck (GLB). This term characterizes the specific difficulty of resolving fine-grained acoustic details that are often semantically sparse or ambiguous when the model is confined to a limited sample space. Lacking access to a broader global semantic context, the model struggles to form robust decision boundaries for long-tail events, leaving a significant portion of the dataset’s semantic potential untapped.

To break this bottleneck, one effective approach is to augment training with an external knowledge base [Dwibedi et al., 2021, Khandelwal et al., 2019, Guu et al., 2020]. However, utilizing external memory introduces synchronization latency between the evolving model and the stored representations [Xiong et al.]. We formalize this temporal discrepancy in our continu-

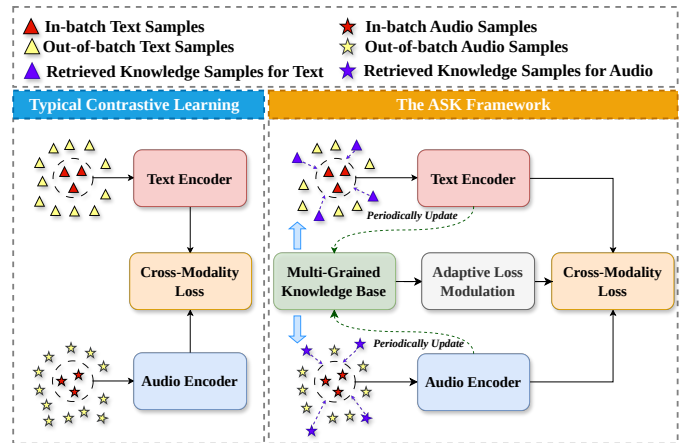


Figure 1: Comparison between typical contrastive learning (left) and our proposed ASK framework (right) with a periodically updated knowledge base and an adaptive loss modulation module.

*Equal contribution.

†Corresponding author.

ous training framework as the Representation-Drift Mismatch (RDM). RDM describes the inevitable lag where audio and

text encoders update rapidly while the external knowledge base remains static or updates slowly. Consequently, the retrieved knowledge risks degrading from a source of semantic guidance into representational noise, potentially destabilizing the training process.

To systematically address these formally defined challenges, we propose the **Adaptive Self-improving Knowledge (ASK)** framework. Uniquely designed as a model-agnostic enhancement, ASK can be seamlessly integrated into various backbones. As shown in Figure 1 (right), it serves as a holistic solution to inject information from a dynamically maintained multi-grained knowledge base. To handle the inherent noise and ambiguity described by the GLB, we introduce an adaptive reliability mechanism that modulates the learning signal based on cross-modal consistency. Simultaneously, to resolve the RDM, ASK employs a dynamic refinement strategy that periodically updates the knowledge base, ensuring that the external guidance co-evolves with the model.

This synergistic design enables ASK to effectively leverage global semantic structures while maintaining training stability, independent of the specific underlying architecture. Extensive experiments across multiple datasets and backbone models demonstrate that our approach consistently achieves state-of-the-art performance, validating the universality and effectiveness of our framework in handling global optimization challenges.

Our main contributions are summarized as follows:

- We identify and define two fundamental challenges in Audio-Text Retrieval: the Gradient Locality Bottleneck (GLB), and the Representation-Drift Mismatch (RDM).
- We propose the Adaptive Self-improving Knowledge (ASK) framework, a model-agnostic solution. It breaks the GLB via multi-grained knowledge injection and systematically mitigates RDM through dynamic knowledge refinement. Furthermore, we introduce a novel adaptive reliability weighting scheme to explicitly filter retrieval noise based on cross-modal consistency.
- Extensive experiments across multiple benchmarks demonstrate that ASK consistently achieves new state-of-the-art performance across diverse global and local interaction architectures. Comprehensive ablation and zero-shot studies further validate the robustness of our framework.

2 Related Work

2.1 Feature Representations

Feature representation serves as the cornerstone of audio-text retrieval. Early Audio-Text Retrieval systems relied on pairing handcrafted acoustic features like MFCCs [Huizen and Kurniati, 2021] with static word embeddings such as Word2Vec [Mikolov et al., 2013]. The advent of deep learning has led to the adoption of powerful, pre-trained unimodal encoders. Text representations are now predominantly extracted from large language models like BERT [Devlin et al., 2019], while audio features are derived from deep models pre-trained on large-scale audio datasets, such as PANNs [Kong et al., 2020] and AST [Gong et al., 2021]. More recently, the field has shifted towards large-scale cross-modal pre-training. Models like CLAP

[Zhao et al., 2023, Guzhov et al., 2022] leverage contrastive learning on vast audio-text datasets to directly learn a shared embedding space, significantly enhancing zero-shot capabilities. Our work builds upon these advanced encoders, proposing a novel mechanism to further enhance their representations during downstream fine-tuning.

2.2 Cross-Modal Interaction and Alignment

Cross-modal interaction is key to achieving semantic alignment in ATR. Early and prevalent approaches perform this at a global, sentence-level, using contrastive learning to align the final embeddings of entire audio clips and text descriptions [Radford et al., 2021, Wu et al., 2022, Mei et al., 2022]. To capture more fine-grained relationships, recent works have focused on local, token-level interactions. These methods typically employ attention mechanisms or cross-modal Transformers to model correspondences between audio frames and text tokens [Lee et al., 2018, Lu et al., 2019, Xie et al., 2024, Yin et al., 2025]. Our ASK framework is orthogonal to these design choices; it operates on the representations themselves and can be seamlessly integrated with both global and local interaction architectures.

2.3 Retrieval-Augmented Contrastive Learning

The challenges formalized as GLB and RDM parallel fundamental bottlenecks in computer vision and information retrieval. To overcome limited in-batch negatives, frameworks like MoCo He et al. [2020] and RocketQA Qu et al. [2021] expand the contrastive denominator via memory queues, while NNCLR Dwivedi et al. [2021] utilizes external support sets. Furthermore, ANCE Xiong et al. proposes asynchronous updates to mitigate stale indices. However, these classical paradigms rely on unimodal queues or strict hard negative mining, making them highly susceptible to acoustic confusion in ATR. Unlike them, ASK structurally breaks the GLB by directly injecting out-of-batch knowledge into representations. Furthermore, to combat the subsequent representation drift, ASK introduces an adaptive reliability weighting scheme that explicitly evaluates cross-modal consistency to filter out retrieval noise.

3 Problem Formulation and Analysis

3.1 Preliminaries

In a standard Audio-Text Retrieval framework, a dual-encoder architecture, comprising an audio encoder $f_\theta(\cdot)$ and a text encoder $g_\phi(\cdot)$, maps an audio-text pair (a_i, t_i) to L2-normalized embeddings u_i and v_i . The encoders are optimized via a symmetric NT-Xent loss [Chen et al., 2020] over a mini-batch B . For a single view, the loss is:

$$\mathcal{L}_i = -\log \frac{\exp(u_i^\top v_i / \tau)}{\sum_{v_j \in B} \exp(u_i^\top v_j / \tau)}, \quad (1)$$

where τ is a temperature hyperparameter. Crucially, as shown in Eq. 1, the contrastive denominator is computed exclusively over samples within the mini-batch B . This inherent structural confinement is the direct cause of the bottleneck we analyze next.

3.2 The Gradient Locality Bottleneck

The batch-centric nature of standard contrastive objectives creates a fundamental limitation in Audio-Text Retrieval. To formalize this, we introduce the concept of **Out-of-Batch Influence (OBI)**, which measures the gradient contribution from data points outside the current mini-batch to the optimization process. Let \mathcal{D} denote the entire training dataset and $B \subset \mathcal{D}$ represent a specific mini-batch. For a batch loss \mathcal{L}_B , the OBI is defined as the expected gradient norm with respect to all out-of-batch embeddings:

$$\text{OBI}(\mathcal{L}_B) = \mathbb{E}_{k \in \mathcal{D} \setminus B} \left[\left\| \frac{\partial \mathcal{L}_B}{\partial u_k} \right\|_2 + \left\| \frac{\partial \mathcal{L}_B}{\partial v_k} \right\|_2 \right], \quad (2)$$

where u_k and v_k are the audio and text embeddings of an out-of-batch sample $k \in \mathcal{D} \setminus B$.

We argue that a training paradigm suffers from a **Gradient Locality Bottleneck (GLB)** if its OBI is identically zero, indicating that no gradient flow exists from out-of-batch data to guide the current optimization step. In a standard ATR framework using the symmetric NT-Xent loss (Eq. 1), the objective \mathcal{L}_B is formulated exclusively as a function of the in-batch embeddings $\{u_j, v_j\}_{j \in B}$. Consequently, the partial derivatives with respect to any out-of-batch embedding u_k or v_k (where $k \notin B$) are necessarily zero:

$$\forall k \in \mathcal{D} \setminus B: \quad \frac{\partial \mathcal{L}_B}{\partial u_k} = \mathbf{0}, \quad \frac{\partial \mathcal{L}_B}{\partial v_k} = \mathbf{0}. \quad (3)$$

This directly results in $\text{OBI}(\mathcal{L}_B) = 0$, proving that standard ATR optimization is strictly constrained by the GLB and cannot leverage the vast semantic information present in out-of-batch data.

This structural confinement prevents the model from leveraging the vast semantic knowledge present in the majority of the dataset. This leads to two critical failures: (1) Semantic Ambiguity and Acoustic Hallucination, where the lack of diverse out-of-batch context prevents the model from learning fine-grained acoustic distinctions between similar but semantically distinct events; and (2) Long-tail Concept Collapse, as the reliance on limited in-batch negatives hinders the formation of robust decision boundaries for rare events, causing the model to default to common concepts with shared tonal properties.

3.3 The Representation Drift Mismatch

A direct approach to break the GLB is to perform knowledge injection, where out-of-batch samples are retrieved and fused with the current samples. By employing a simple feature fusion such as $u'_i = (1 - \rho)u_i + \rho\mathcal{K}$, where u_i is the embedding of the current sample, \mathcal{K} is the retrieved out-of-batch knowledge and ρ represents the injection ratio, we establish a non-zero gradient pathway from the out-of-batch data to the model parameters. This ensures that the Out-of-Batch Influence (OBI) is no longer zero, effectively breaking the structural confinement of standard contrastive learning.

While knowledge injection breaks the GLB by introducing out-of-batch samples $\mathcal{D} \setminus B$, it inherently introduces a critical challenge: **Representation Drift Mismatch (RDM)**. Since the encoders f_{θ_t} and g_{θ_t} are non-stationary and evolve during optimization, a static knowledge base constructed at step t_k becomes

progressively misaligned with the current model state at step t ($t > t_k$). To formalize this, taking the audio modality as an example, we define RDM as the expected Kullback-Leibler (KL) divergence [Kullback and Leibler \[1951\]](#) between the ideal neighborhood distribution P_{ideal} and the actual distribution P_{actual} :

$$\begin{aligned} \text{RDM}(t, t_k) &= \mathbb{E}_{a_i \in \mathcal{D}} [D_{\text{KL}}(P_{\text{ideal}}(\cdot|i) \| P_{\text{actual}}(\cdot|i))], \\ P_{\text{ideal}}(j|i) &\propto \exp(\text{sim}(f_{\theta_t}(a_i), f_{\theta_t}(a_j))), \\ P_{\text{actual}}(j|i) &\propto \exp(\text{sim}(f_{\theta_t}(a_i), f_{\theta_{t_k}}(a_j))), \end{aligned} \quad (4)$$

where a_i denotes the current query sample, the distributions are normalized over all knowledge samples indexed by j , θ_t and θ_{t_k} represent the model parameters at the current step t and the knowledge snapshot step t_k respectively, and $\text{sim}(\cdot, \cdot)$ is the dot product similarity.

Formally, the knowledge vector \mathcal{K} is computed as the expected representation over the neighborhood distribution: $\mathcal{K} = \sum_j P(j)z_j$, where z_j denotes the embedding of the j -th knowledge sample. As the training progresses, RDM accumulates and corrupts the optimization objective by inducing a deviation in the fused knowledge vectors \mathcal{K} , $\Delta\mathcal{K} = \mathcal{K}_{\text{actual}} - \mathcal{K}_{\text{ideal}}$.

The impact of this drift on training stability can be quantified via the gradient deviation: $\Delta\nabla = \nabla_{\theta_t} \mathcal{L}_{\text{actual}} - \nabla_{\theta_t} \mathcal{L}_{\text{ideal}}$. Specifically, consider a simplified loss: $\mathcal{L} = \mathcal{L}_{\text{main}}(u_i, u'_i)$ that incorporates the knowledge-enhanced representation: $u'_i = (1 - \rho)u_i + \rho\mathcal{K}$. The gradient with respect to parameters θ_t is: $\nabla_{\theta_t} \mathcal{L} = \left(\frac{\partial \mathcal{L}}{\partial u_i} + (1 - \rho) \frac{\partial \mathcal{L}}{\partial u'_i} \right) \frac{\partial u_i}{\partial \theta_t}$. By performing a first-order Taylor expansion of the loss derivative around the ideal representation, we obtain:

$$\frac{\partial \mathcal{L}_{\text{actual}}}{\partial u'_i} - \frac{\partial \mathcal{L}_{\text{ideal}}}{\partial u'_i} \approx H_{\mathcal{L}}(u'_{\text{ideal}}) \cdot \rho \Delta\mathcal{K}, \quad (5)$$

where $H_{\mathcal{L}}$ is the Hessian matrix. This proves that the gradient misalignment $\Delta\nabla$ is approximately proportional to the knowledge deviation $\Delta\mathcal{K}$. To bound this deviation, we leverage Pinsker's inequality to relate the KL divergence to the Total Variation Distance, yielding the relationship:

$$\|\Delta\mathcal{K}\|_2 \leq C \sqrt{2 \cdot \text{RDM}(t, t_k)}, \quad (6)$$

where $C = \max_j \|z_j\|_2$ is a bounded constant. Equation 6 establishes a formal link between RDM and the potential error margin for the gradients. Higher RDM directly widens this margin, causing training instability and representational noise. This theoretical foundation necessitates our dynamic refinement mechanism, which periodically resets the RDM to zero to ensure stable co-evolution between the model and its knowledge.

4 The Adaptive Self-improving Knowledge Framework

In this section, we elaborate on each component of our proposed framework ASK, whose architecture is shown in Figure 2.

4.1 Formulation of Knowledge Bases

Our framework's first step is to construct multi-grained knowledge bases from a source dataset, \mathcal{D}_k . The choice of source is flexible; in our experiments, we explore three types

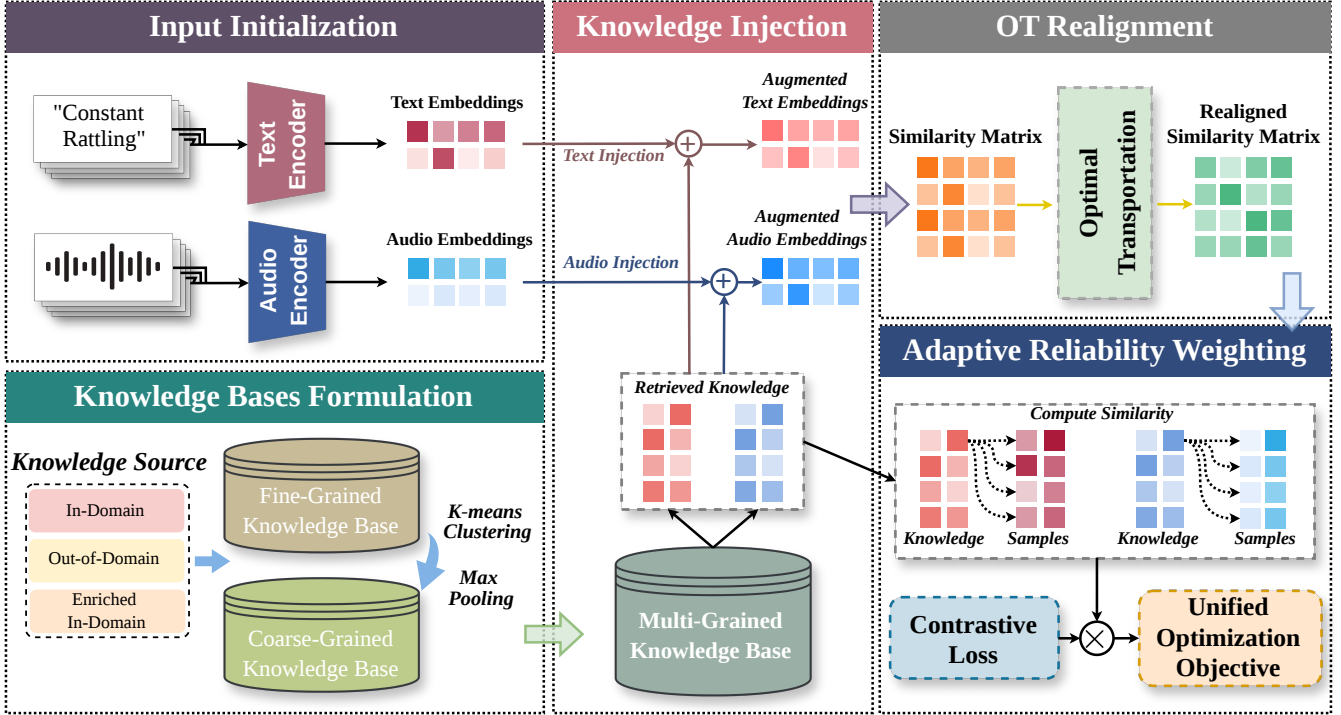


Figure 2: The proposed ASK framework. A multi-grained knowledge base is periodically updated to mitigate RDM. During training, knowledge is injected into samples, and a cross-modal reliability weight is computed. A final loss is optimized using both an OT-realigned similarity matrix and the reliability weight.

to demonstrate versatility: 1) In-Domain⁺: the training set itself, 2) Out-of-Domain[†]: WavCaps [Mei et al., 2024], and 3) Enriched In-Domain^{*}: training set re-annotated by Gemini 2.5 [Comanici et al., 2025]. From a chosen source, we construct two complementary bases.

Fine-Grained Knowledge Base. The fine-grained base, K_f , captures instance-level semantic details. It is formed by encoding all audio-text pairs in the source $\mathcal{D}_k = \{(a_j^k, t_j^k)\}_{j=1}^{N_k}$ using the current model encoders $f_\theta(\cdot)$ and $g_\phi(\cdot)$. The result is a collection of L2-normalized embedding pairs:

$$K_f = \{(u_j^k, v_j^k)\}_{j=1}^{N_k}, \quad (7)$$

where $u_j^k = f_\theta(a_j^k)$, $v_j^k = g_\phi(t_j^k)$.

Coarse-Grained Knowledge Base. The coarse-grained base, K_c , provides a global semantic prior by storing a set of learned prototypes. These prototypes are generated by first partitioning the fine-grained embeddings via K-Means clustering into N_c groups, and then distilling the salient features from each group. For the m -th audio cluster C_m^u , which contains all member embeddings $\{u_j^k\}$, its prototype c_m^u is computed via max-pooling:

$$c_m^u = \text{MaxPooling}(\{u_j^k \mid u_j^k \in C_m^u\}). \quad (8)$$

An identical procedure is applied to the text embeddings to yield text prototypes $\{c_m^v\}_{m=1}^{N_c}$. The final coarse-grained base is the set of these prototype pairs, $K_c = \{(c_m^u, c_m^v)\}_{m=1}^{N_c}$.

4.2 Multi-Grained Knowledge Injection

With the knowledge bases established, we perform two parallel injection processes to create distinct fine-grained and coarse-grained enhanced embeddings for each training sample.

For the fine-grained injection, we first retrieve the Top-K nearest neighbors for a given embedding (e.g., audio u_i) from K_f , yielding the neighborhood set $\mathcal{N}_f(u_i)$. The retrieved embeddings are averaged to form a knowledge vector \bar{u}_i^f , which is then interpolated with the original embedding u_i :

$$u'_{i,f} = (1 - \rho)u_i + \rho\bar{u}_i^f, \quad (9)$$

$$\bar{u}_i^f = \frac{\sum_{(u_j^k, v_j^k) \in \mathcal{N}_f(u_i)} u_j^k}{K},$$

where ρ is an interpolation hyperparameter. An identical, parallel process is performed using the coarse-grained base K_c to produce the coarse-grained enhanced representation, $u'_{i,c}$. A symmetric procedure is applied to the text embedding v_i , ultimately yielding two distinct sets of enhanced embedding pairs for the final optimization: $(u'_{i,f}, v'_{i,f})$ and $(u'_{i,c}, v'_{i,c})$.

Breaking the Gradient Locality Bottleneck. This injection mechanism breaks the GLB (Sec. 3.2) by creating a gradient pathway to out-of-batch knowledge. For any out-of-batch knowledge item u_k^k retrieved by an in-batch sample u_i , its gradient is non-zero. Let $\mathcal{S}_k = \{i \in B \mid u_k^k \in \mathcal{N}_f(u_i)\}$ be the set of in-batch samples that retrieved u_k^k . The gradient of the loss \mathcal{L}'_B w.r.t. u_k^k

is:

$$\frac{\partial \mathcal{L}'_B}{\partial u_k^k} = \sum_{i \in S_k} \frac{\partial \mathcal{L}'_B}{\partial u'_{i,f}} \frac{\partial u'_{i,f}}{\partial u_k^k}. \quad (10)$$

From Eq. 9, the second partial derivative is a non-zero constant $\frac{\rho}{K}$. Given that one of its partial derivatives is non-zero, the total gradient is therefore non-zero. Consequently, the OBI, defined in Eq. 2, becomes strictly positive. This quantitatively proves that our injection process breaks the GLB.

4.3 Adaptive Reliability Weighting

To mitigate the risk of injecting noisy knowledge from equally-weighted neighbors (Sec. 4.2), we introduce an adaptive weighting mechanism. This mechanism is based on the principle of cross-modal consistency: for a well-aligned audio-text pair (u_i, v_i) , the neighborhoods retrieved by u_i and v_i should themselves be semantically consistent. We quantify this consistency to compute a reliability score for each neighbor, which in turn modulates its contribution to the final objective.

Fine-Grained Reliability Weighting. For each pair (u_i, v_i) , we consider two fine-grained neighborhoods: the audio-retrieved audio set $\mathcal{U}_r = \{u_i^k\}_{k=1}^K$ and the text-retrieved audio-text set $\mathcal{N}_f(v_i) = \{(u_j^k, v_j^k)\}_{j=1}^K$. We first assign each neighbor in $\mathcal{N}_f(v_i)$ a consistency score \bar{s}_j , defined as its average similarity to the audio-retrieved neighborhood:

$$\bar{s}_j = \frac{1}{K} \sum_{l=1}^K (u_j^k)^\top u_l^k. \quad (11)$$

These scores are subsequently normalized via a softmax function to yield the reliability weights $\mathbf{w}_f = \{w_j\}_{j=1}^K$:

$$w_j = \frac{\exp(\bar{s}_j)}{\sum_{m=1}^K \exp(\bar{s}_m)}. \quad (12)$$

The reliability-aware knowledge potential is then computed as the weighted similarity between u_i and the audio components of $\mathcal{N}_f(v_i)$:

$$\Psi_{i,f}^{T \rightarrow A} = \sum_{j=1}^K w_j \cdot \exp(u_i^\top u_j^k). \quad (13)$$

A symmetric construction produces the text-side potential $\Psi_{i,f}^{A \rightarrow T}$, based on the audio-retrieved text neighborhood.

Coarse-Grained Reliability Weighting. An identical procedure is applied to the coarse-grained neighborhoods to produce the coarse-grained potentials, $\Psi_{i,c}^{T \rightarrow A}$ and $\Psi_{i,c}^{A \rightarrow T}$. These potentials represent the model’s alignment with reliable, high-level semantic prototypes.

The resulting four reliability-aware potentials are core components that will be directly incorporated into our final optimization objective, as detailed in Section 4.5.

4.4 Dynamic Knowledge Refinement

As shown in Section 3.3, a static knowledge base leads to Representation Drift Mismatch (RDM), which induces increasing gradient misalignment during training. To mitigate this,

we employ a dynamic refinement mechanism that periodically reconstructs the knowledge bases K_f and K_c using the current encoders. The update period \mathcal{T} specifies the number of epochs between successive reconstructions.

This procedure directly controls the RDM. At each update step t , refinement sets the knowledge-base timestamp to $t_k = t$, making the ideal and actual neighborhood distributions identical, $P_{\text{ideal}} \equiv P_{\text{actual}}$. Thus, the RDM (Eq. 4) is reset to its minimum value:

$$\text{RDM}(t, t) = \mathbb{E}[D_{KL}(P_{\text{ideal}} \| P_{\text{ideal}})] = 0. \quad (14)$$

By periodically driving the RDM to zero, the mechanism also resets the upper bound on gradient deviation (Eq. 6), ensuring stable optimization and enabling the knowledge base to co-evolve with the model.

4.5 Unified Optimization Objective

The final optimization objective is constructed in two main stages. First, we compute NT-Xent losses on similarity matrices that have been realigned via Optimal Transport. Second, these losses are modulated by our reliability-aware knowledge potentials to form the final composite objective.

Loss on OT-Realigned Similarities. The process begins with the knowledge-enhanced embeddings from Section 4.2. For a mini-batch, we compute a fine-grained similarity matrix \mathbf{S}_f and a coarse-grained one \mathbf{S}_c . Since the audio and text knowledge are retrieved independently, the distributions of their nearest neighbors within the batch may differ. To reconcile this potential discrepancy and find a globally optimal batch-level matching, we employ Optimal Transport (OT) [Cuturi, 2013] to learn an optimal transport plan \mathbf{Q}^* . This plan is then used to produce the realigned similarity matrices \mathbf{S}_f^* and \mathbf{S}_c^* :

$$\mathbf{S}_f^* = ((1 - \beta)\mathbf{I} + \beta\mathbf{Q}^*)\mathbf{S}_f. \quad (15)$$

An identical process is applied to \mathbf{S}_c . Based on these realigned matrices, we define two NT-Xent loss components. The text-to-audio loss, $\mathcal{L}_{T \rightarrow A}$, is the sum of the fine- and coarse-grained objectives:

$$\begin{aligned} \mathcal{L}_{T \rightarrow A} = & -\frac{1}{B} \sum_{i=1}^B \log \frac{\exp((\mathbf{S}_f^*)_{ii}/\tau)}{\sum_{j=1}^B \exp((\mathbf{S}_f^*)_{ij}/\tau)} \\ & -\frac{1}{B} \sum_{i=1}^B \log \frac{\exp((\mathbf{S}_c^*)_{ii}/\tau)}{\sum_{j=1}^B \exp((\mathbf{S}_c^*)_{ij}/\tau)}. \end{aligned} \quad (16)$$

The audio-to-text loss, $\mathcal{L}_{A \rightarrow T}$, is formulated symmetrically.

Reliability-Aware Objective. The OT-realigned losses above do not yet account for the cross-modal consistency of the retrieved knowledge. To incorporate this, we use the knowledge potentials computed in Section 4.3 as reliability modulators. We first define the reliability-aware terms, e.g., for the text-to-audio direction:

$$\begin{aligned} \mathcal{F}_f^{T \rightarrow A} &= \frac{1}{|B|} \sum_{i=1}^{|B|} -\log \Psi_{i,f}^{T \rightarrow A}, \\ \mathcal{F}_c^{T \rightarrow A} &= \frac{1}{|B|} \sum_{i=1}^{|B|} -\log \Psi_{i,c}^{T \rightarrow A}. \end{aligned} \quad (17)$$

The final text-to-audio loss, $\mathcal{L}_{T \rightarrow A}^*$, is then the base OT-realigned loss, modulated by a weighted sum of these reliability terms:

$$\mathcal{L}_{T \rightarrow A}^* = (1 + \lambda_f \mathcal{F}_f^{T \rightarrow A} + \lambda_c \mathcal{F}_c^{T \rightarrow A}) \cdot \mathcal{L}_{T \rightarrow A}, \quad (18)$$

where λ_f and λ_c are hyperparameters. The final audio-to-text loss, $\mathcal{L}_{A \rightarrow T}^*$, is computed symmetrically. The overall loss for the ASK framework is the average of these two modulated objectives:

$$\mathcal{L}_{\text{ASK}} = \frac{1}{2}(\mathcal{L}_{T \rightarrow A}^* + \mathcal{L}_{A \rightarrow T}^*). \quad (19)$$

This composite objective ensures the model learns from multi-grained knowledge that is both globally aligned at the batch level and weighted by its cross-modal reliability.

4.6 Theoretical Analysis

We provide a theoretical justification for ASK, framing the training as an alternating optimization to maximize the log-likelihood of observed audio-text pairs $x_i = (a_i, t_i)$.

Probabilistic Formulation via ELBO Our goal is to maximize the log-likelihood $\mathcal{L}(\theta) = \sum_i \log p(x_i; \theta)$. By introducing latent variables $z_i = (z_{i,f}, z_{i,c})$ representing the optimal knowledge, and an auxiliary distribution $Q(z_i)$, we apply Jensen’s Inequality to derive the Evidence Lower Bound (ELBO), $\mathcal{F}(Q, \theta)$:

$$\begin{aligned} \mathcal{L}(\theta) &= \sum_i \log \sum_{z_i} \frac{p(x_i, z_i; \theta)}{Q(z_i)} Q(z_i) \\ &\geq \sum_i \mathbb{E}_{Q(z_i)} [\log p(x_i, z_i; \theta)] + H(Q) \triangleq \mathcal{F}(Q, \theta), \end{aligned} \quad (20)$$

where $H(Q)$ is the entropy and maximizing $\mathcal{L}(\theta)$ is achieved by iteratively maximizing $\mathcal{F}(Q, \theta)$.

Alternating Optimization. Let θ_t be the parameters at iteration t . The process alternates between two stages:

Stage 1: Auxiliary Distribution Update. Fixing θ_t , we approximate the optimal $Q_t(z_i)$ using the retrieved neighbors. We define the probability mass of Q_t over a neighbor z_j directly via our reliability weights (Eq. 12): $Q_{t,f}(z_j) := w_{j,f}(\theta_t)$ and $Q_{t,c}(z_j) := w_{j,c}(\theta_t)$.

Stage 2: Model Parameter Update. Fixing Q_t , we maximize the expectation $\mathbb{E}_{Q_t}[\log p(x_i, z_i; \theta)]$. We model the joint log-probability as the negative sum of the alignment loss and the reliability potential: $\log p(x_i, z_i; \theta) \propto -(\mathcal{L}_{OT}(\theta) + \log \Psi_i(\theta))$. Substituting this into the ELBO, the maximization objective becomes minimizing the negative expectation:

$$\min_{\theta} \mathcal{L}_m \approx \sum_i \left(\mathbb{E}_{Q_{t,f}} [\mathcal{L}_{OT,f} + \log \Psi_{i,f}] + \mathbb{E}_{Q_{t,c}} [\mathcal{L}_{OT,c} + \log \Psi_{i,c}] \right). \quad (21)$$

This objective \mathcal{L}_m mathematically aligns with our modulated loss \mathcal{L}^* (Eq. 18), where the reliability term $\mathcal{F} = -\log \Psi$ acts as a regularizer.

Convergence. Since each step monotonically increases the ELBO $\mathcal{F}(Q, \theta)$, and \mathcal{L}_{ASK} is bounded below, the Monotone Convergence Theorem guarantees that the sequence of loss values converges to a stationary point.

5 Experiments

5.1 Experimental Setup

Datasets and Metrics. We evaluate our method on two standard benchmarks: AudioCaps [Kim et al., 2019] and Clotho [Drossos et al., 2020]. Following prior work [Mei et al., 2022, Xie et al., 2024, Yan et al., 2024], we report audio-to-text (A2T) and text-to-audio (T2A) retrieval performance using Recall at K (R@K, for K=1, 5, 10).

Baselines. To validate ASK’s model-agnosticism, we evaluate it across two interaction paradigms. **1) Global Interaction:** We build upon the ML-ACT baseline [Mei et al., 2022] (ResNet-38 [Kong et al., 2020] + BERT [Devlin et al., 2019]), comparing against BLAT [Xu et al., 2023] and Auto-ACD [Sun et al., 2024]. We also adapt the English-only ML-CLAP setup [Yan et al., 2024] (CED-Base [Dinkel et al., 2024] + SONAR-TE [Duquenne et al., 2023]), comparing it with GLAP [Dinkel et al., 2025]. **2) Local Interaction:** We follow the setups of GPA [Xie et al., 2024] and FLAM [Wu et al.], and adopt the same maximum number of tokens for the dataset.

Implementation Details. All models are trained with the Adam optimizer [Kingma and Ba, 2014]. The ResNet-BERT architecture is trained for 50 epochs on AudioCaps (batch size 32) and Clotho (batch size 24), with an initial learning rate of 5×10^{-5} , which is decayed by a factor of 10 every 20 epochs. The CED-SONAR models are trained for 10 epochs with a decay step applied every 4 epochs. We use the Faiss library [Douze et al., 2025] for efficient neighbor search. Unless specified otherwise, the hyperparameters for our ASK framework are set as follows: we retrieve $K = 10$ neighbors, with a coarse-grained prototype set of size $N_c = 512$. The knowledge injection ratio is $\rho = 0.2$, and the OT-realignment factor is $\beta = 0.2$. Empirical analyses confirm our framework’s robustness across $K \in [5, 15]$ and $\rho \in [0.15, 0.25]$. The reliability modulation weights are $\lambda_f = 0.2$ and $\lambda_c = 0.3$. The knowledge base is dynamically refined every $\mathcal{T} = 15$ epochs. All experiments were conducted on 2 NVIDIA A100 and 8 RTX 4090 GPUs.

5.2 Main Results

We evaluate the effectiveness of our proposed ASK framework by integrating it into various baseline models. The results are organized by the cross-modal interaction strategy.

Global Interaction Strategy. Table 1 presents the results for models using a global, sentence-level interaction strategy. ASK consistently outperforms competitive methods across all datasets and architectures. On AudioCaps (ResNet-BERT), ASK surpasses the foundational ML-ACT by a remarkable 6.0% (A2T) and 3.2% (T2A) in absolute R@1. Crucially, it eclipses Auto-ACD, with further R@1 gains of up to 1.5% (ASK[†]) and 2.2% (ASK⁺). These improvements validate our core mechanisms in successfully breaking the GLB and mitigating RDM. Demonstrating its model-agnosticism, ASK also significantly enhances the transformer-based CED-SONAR architecture. On the Clotho dataset, it outperforms the GLAP baseline, boosting A2T R@1 to 19.7% (+1.3%) and T2A R@1 to 16.3% (+1.2%). Finally, the varying optimal variants across setups highlight ASK’s flexibility in leveraging diverse knowledge sources.

Table 1: Results for Audio-Text-Retrieval on AudioCaps and Clotho under the global interaction strategy. The symbols \dagger , $*$, and $+$ denote the use of knowledge from WavCaps, the Gemini-annotated training set and the original training set respectively.

Method	AudioCaps						Clotho					
	Audio-to-Text			Text-to-Audio			Audio-to-Text			Text-to-Audio		
	R@1	R@5	R@10	R@1	R@5	R@10	R@1	R@5	R@10	R@1	R@5	R@10
Architecture: ResNet-38 + BERT												
ML-ACT Mei et al. [2022]	36.3 \pm 0.5	68.6 \pm 0.3	81.5 \pm 0.2	32.2 \pm 0.4	68.2 \pm 0.1	81.2 \pm 0.2	16.3 \pm 0.4	39.1 \pm 0.3	51.5 \pm 0.6	14.2 \pm 0.4	37.3 \pm 0.2	49.9 \pm 0.3
BLAT Xu et al. [2023]	38.2 \pm 0.2	70.4 \pm 0.3	82.1 \pm 0.2	32.9 \pm 0.3	68.9 \pm 0.1	81.8 \pm 0.2	16.8 \pm 0.2	39.6 \pm 0.3	52.1 \pm 0.3	14.1 \pm 0.2	37.6 \pm 0.2	50.2 \pm 0.1
Auto-ACD Sun et al. [2024]	40.8 \pm 0.2	71.3 \pm 0.4	83.3 \pm 0.2	33.2 \pm 0.3	68.7 \pm 0.2	82.1 \pm 0.2	17.1 \pm 0.2	39.3 \pm 0.2	53.2 \pm 0.3	14.4 \pm 0.2	37.5 \pm 0.2	50.1 \pm 0.2
ASK \dagger	42.3 \pm 0.3	73.3 \pm 0.8	84.2 \pm 0.6	34.6 \pm 0.5	69.6 \pm 0.4	82.9 \pm 0.9	17.3 \pm 0.3	40.2 \pm 0.6	54.1 \pm 0.2	14.8 \pm 0.4	38.1 \pm 0.7	50.7 \pm 0.6
ASK $*$	39.5 \pm 0.3	73.2 \pm 0.4	85.3 \pm 0.6	34.2 \pm 0.6	69.1 \pm 0.7	81.9 \pm 0.3	18.5 \pm 0.2	40.1 \pm 0.4	53.6 \pm 0.6	14.7 \pm 0.5	38.3 \pm 0.9	50.1 \pm 0.3
ASK $+$	42.0 \pm 0.2	74.2 \pm 0.5	85.4 \pm 0.6	35.4 \pm 0.3	70.2 \pm 0.3	83.1 \pm 0.7	17.5 \pm 0.2	40.3 \pm 0.8	54.1 \pm 0.6	15.2 \pm 0.3	38.5 \pm 0.6	51.1 \pm 0.4
Architecture: CED-Base + SONAR-TE												
ML-CLAP Yan et al. [2024]	39.6 \pm 0.2	69.8 \pm 0.3	81.7 \pm 0.6	31.9 \pm 0.3	69.2 \pm 0.5	82.8 \pm 0.9	18.0 \pm 0.2	39.5 \pm 0.7	53.0 \pm 0.6	14.9 \pm 0.3	39.9 \pm 0.6	53.1 \pm 0.7
GLAP Dinkel et al. [2025]	41.2 \pm 0.1	72.4 \pm 0.3	83.7 \pm 0.2	33.3 \pm 0.3	68.9 \pm 0.1	81.8 \pm 0.4	18.4 \pm 0.2	40.6 \pm 0.3	54.1 \pm 0.3	15.1 \pm 0.2	40.2 \pm 0.2	54.2 \pm 0.1
ASK \dagger	43.3 \pm 0.3	73.7 \pm 0.6	84.4 \pm 0.8	34.8 \pm 0.2	70.6 \pm 0.5	84.0 \pm 0.4	19.0 \pm 0.1	41.5 \pm 0.6	56.5 \pm 0.7	16.3 \pm 0.2	40.3 \pm 0.6	55.4 \pm 0.7
ASK $*$	41.9 \pm 0.3	74.1 \pm 0.4	85.6 \pm 0.6	34.9 \pm 0.2	70.9 \pm 0.5	84.1 \pm 0.7	18.5 \pm 0.2	41.6 \pm 0.6	56.9 \pm 0.7	16.0 \pm 0.1	40.6 \pm 0.5	55.1 \pm 0.8
ASK $+$	40.9 \pm 0.2	71.6 \pm 0.6	84.3 \pm 0.3	33.7 \pm 0.2	70.3 \pm 0.5	83.5 \pm 0.6	19.7 \pm 0.1	43.3 \pm 0.5	57.3 \pm 0.7	16.0 \pm 0.2	41.5 \pm 0.6	55.2 \pm 0.7

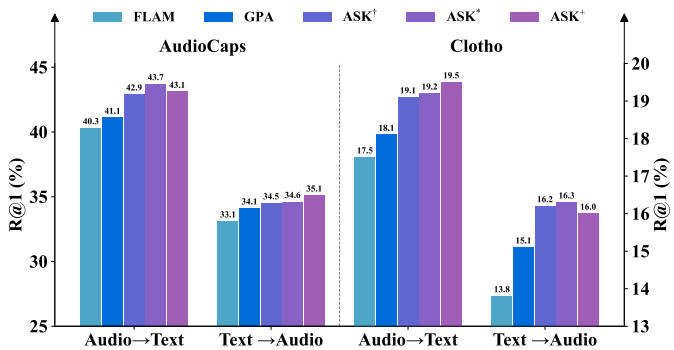


Figure 3: Results for Audio-Text Retrieval on AudioCaps and Clotho under the local interaction strategy. The symbols \dagger , $+$, and $*$ denote different knowledge sources in Section 4.1.

Local Interaction Strategy. We also validate ASK with local, token-level interaction strategies [Xie et al., 2024, Wu et al.]. Figure 3 presents the retrieval results for our local, token-level interaction baselines. The results demonstrate consistent and significant gains across both retrieval directions, outperforming both the FLAM and GPA baselines. On AudioCaps, ASK achieves substantial improvements over the strongest baseline (GPA), with ASK $*$ enhancing the Audio-to-Text R@1 by 2.6% and ASK $+$ boosting the Text-to-Audio R@1 by 1.0%. On Clotho, ASK $+$ delivers the top Audio-to-Text R@1 performance, while ASK $*$ yields the best Text-to-Audio R@1. Notably, our variants exceed FLAM by even larger margins across all metrics. These symmetric improvements confirm the universal benefit of our framework.

Zero-Shot Generalization. To strictly evaluate robustness, we conduct bidirectional zero-shot experiments: training on AudioCaps and testing on Clotho, and vice versa. As illustrated in Figure 4, the ASK framework consistently expands the retrieval performance envelope compared to the baseline across all metrics in both transfer directions. Specifically, when trans-

ferring from AudioCaps to Clotho (left), leveraging the diverse WavCaps knowledge source (ASK \dagger) yields a notable 1.3% absolute gain in A2T R@1. Similarly, in the Clotho-to-AudioCaps transfer (right), ASK variants maintain superior performance, with ASK \dagger achieving a significant improvement over the baseline (e.g., +2.6% in A2T R@1). These results confirm that our multi-grained knowledge injection effectively mitigates domain shifts and prevents overfitting to source-domain specifics.

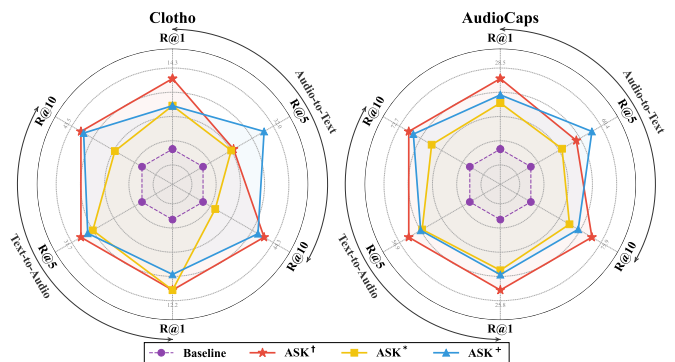


Figure 4: Zero-shot performance on AudioCaps and Clotho. \dagger , $*$, and $+$ denote different knowledge sources in Section 4.1.

5.3 Ablation Study and Analysis

To validate the contribution of each component within our ASK framework, we conduct a series of ablation studies on the AudioCaps dataset using the ResNet-BERT architecture and an in-domain knowledge source. The results are presented in Table 2.

Impact of Multi-Grained Knowledge Bases. We first analyze the necessity of our multi-grained design. Removing the fine-grained knowledge base results in a substantial performance drop of 4.3% absolute in A2T R@1, confirming the critical

Table 2: Ablation experiments on AudioCaps dataset using the ResNet-38 + BERT architecture. ⁺ denotes the utilization of knowledge derived from AudioCaps training set.

G.	Method	A2T			T2A		
		R@1	R@5	R@10	R@1	R@5	R@10
	w/o ASK	36.3 \pm 0.5	68.6 \pm 0.3	81.5 \pm 0.2	32.2 \pm 0.4	68.2 \pm 0.1	81.2 \pm 0.2
1	w/o Fine-grained Knowledge Base	37.7 \pm 0.2	70.4 \pm 0.4	81.8 \pm 0.7	31.9 \pm 0.2	67.3 \pm 0.6	81.0 \pm 0.7
	w/o Coarse-grained Knowledge Base	37.4 \pm 0.1	67.6 \pm 0.5	81.3 \pm 0.7	31.2 \pm 0.3	66.6 \pm 0.4	81.0 \pm 0.6
2	w/o the Knowledge Injection Step	39.1 \pm 0.3	72.7 \pm 0.6	84.1 \pm 0.7	34.5 \pm 0.3	69.1 \pm 0.6	82.6 \pm 0.7
	w/o OT Alignment Correction	41.1 \pm 0.3	73.4 \pm 0.5	85.2 \pm 0.6	34.2 \pm 0.2	69.4 \pm 0.4	82.8 \pm 0.6
3	w/o Adaptive Reliability Weighting	39.3 \pm 0.2	72.2 \pm 0.4	83.6 \pm 0.6	33.9 \pm 0.3	68.9 \pm 0.5	81.6 \pm 0.7
4	w/o the Dynamic Knowledge Refinement	39.2 \pm 0.3	71.0 \pm 0.6	83.8 \pm 0.5	34.1 \pm 0.2	68.7 \pm 0.6	81.5 \pm 0.5
	Our Full ASK⁺	42.0\pm0.2	74.2\pm0.5	85.4\pm0.6	35.4\pm0.3	70.2\pm0.3	83.1\pm0.7

role of instance-level details for precise retrieval. Similarly, removing the coarse-grained base leads to a 4.6% drop in A2T R@1, which underscores the importance of the global semantic prior provided by the prototypes. The model, which leverages both, significantly outperforms either single-granularity variant, demonstrating that the fine- and coarse-grained knowledge sources are complementary.

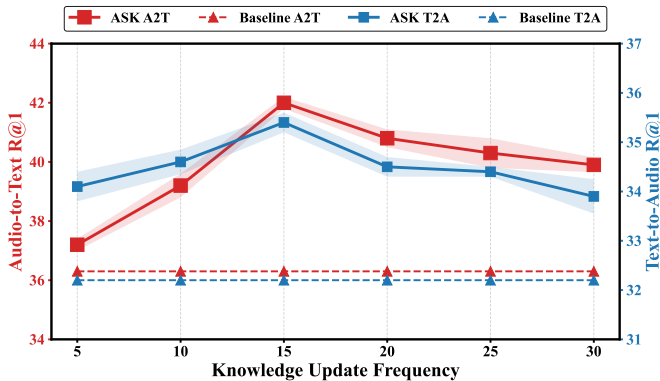


Figure 5: Effect of the frequency \mathcal{T} of Knowledge Update. Ablation experiment on ASK⁺ under the global interaction strategy.

Impact of Core ASK Mechanisms. We then ablate the core mechanisms of ASK. **1) Knowledge Injection:** Disabling the knowledge injection step causes a notable drop of 2.9% in A2T R@1. This empirically validates that creating gradient pathways to out-of-batch data is the primary driver for breaking the GLB and enhancing representations. **2) Reliability Weighting:** Ablating our adaptive reliability weighting mechanism results in a significant 2.7% drop in A2T R@1 and a 1.5% drop in T2A R@1. This provides strong evidence that not all retrieved knowledge is equally beneficial, and that modulating the loss based on cross-modal consistency is crucial for mitigating the impact of noises and achieving robust performance.

Impact of Dynamic Knowledge Refinement. We evaluate the effect of the knowledge-base update period \mathcal{T} on mitigating RDM. As shown in Table 2, disabling dynamic refinement leads to a 2.8% drop in A2T R1, empirically validating our theoretical claim in Section 3.3 that unchecked RDM introduces stale and misaligned knowledge.

Figure 5 shows that performance improves as the update frequency increases, reaching an optimum at $T = 15$ epochs, which surpasses both the static knowledge base and the baseline. However, overly frequent updates degrade performance, indicating a trade-off: while frequent updates curtail RDM, they can also destabilize the knowledge representation before the model fully adapts. These findings highlight the necessity of a co-evolving knowledge base and careful tuning of the update frequency.

Table 3: Qualitative comparison of audio-text retrieval. GT represents Ground Truth.

Audio Query	ML-ACT et al. [2022]	Mei	ASK (Ours)
<i>Scenario 1: Semantic Ambiguity</i>			
GT: “Thunder roars in the distance as rain falls” (Confusing Texture)	Top-1: “Food sizzling in a pan” ✗ (Audio Ambiguity) GT Rank: 21	Top-1: “Thunder roars in the distance as rain falls” ✓ GT Rank: 1	
<i>Scenario 2: Long-tail Concept</i>			
GT: “Church bells ringing” (Rare Event)	Top-1: “Train horn blowing” ✗ (Tonal Similarity) GT Rank: 13	Top-1: “Church bells ringing” ✓ GT Rank: 1	

Case Study. Table 3 qualitatively illustrates how the ASK framework overcomes the Gradient Locality Bottleneck (GLB).

In Scenario 1, the baseline model fails to resolve semantic ambiguity between acoustically similar textures like *thunder* and *sizzling food*, whereas ASK distinguishes these fine-grained details to achieve Rank 1. Likewise, for the long-tail *Church bells* concept, ASK avoids the baseline’s tendency to default to common tonal relatives like *train horns*. These results demonstrate that leveraging diverse out-of-batch knowledge during training allows ASK to learn a discriminative embedding space that generalizes to rare and ambiguous events without requiring explicit retrieval during inference.

6 Conclusion

In this paper, we identified and formalized two fundamental challenges in knowledge-enhanced Audio-Text Retrieval: the Gradient Locality Bottleneck, which confines standard contrastive learning to mini-batches, and the consequent Representation-Drift Mismatch, which arises from using static knowledge bases with evolving models. To address this dual challenge, we proposed the Adaptive Self-improving Knowledge framework. ASK is a model-agnostic, plug-and-play solution that breaks the GLB via multi-grained knowledge injection, mitigates RDM through dynamic knowledge refinement, and ensures reliability with a novel adaptive weighting scheme. Extensive experiments demonstrate that ASK consistently and significantly improves performance across diverse architectures and datasets, achieving new state-of-the-art results.

References

- Ting Chen, Simon Kornblith, Mohammad Norouzi, and Geoffrey Hinton. A simple framework for contrastive learning of visual representations. In *International conference on machine learning*, pages 1597–1607. PmLR, 2020.
- Gheorghe Comanici, Eric Bieber, Mike Schaekermann, Ice Pasupat, Noveen Sachdeva, Inderjit Dhillon, Marcel Blistein, Ori Ram, Dan Zhang, Evan Rosen, et al. Gemini 2.5: Pushing the frontier with advanced reasoning, multimodality, long context, and next generation agentic capabilities. *arXiv preprint arXiv:2507.06261*, 2025.
- Marco Cuturi. Sinkhorn distances: Lightspeed computation of optimal transport. *Advances in neural information processing systems*, 26, 2013.
- Jacob Devlin, Ming-Wei Chang, Kenton Lee, and Kristina Toutanova. Bert: Pre-training of deep bidirectional transformers for language understanding. In *Proceedings of the 2019 conference of the North American chapter of the association for computational linguistics: human language technologies, volume 1 (long and short papers)*, pages 4171–4186, 2019.
- Heinrich Dinkel, Yongqing Wang, Zhiyong Yan, Junbo Zhang, and Yujun Wang. Ced: Consistent ensemble distillation for audio tagging. In *ICASSP 2024-2024 IEEE International Conference on Acoustics, Speech and Signal Processing (ICASSP)*, pages 291–295. IEEE, 2024.
- Heinrich Dinkel et al. Glap: General contrastive audio–text pretraining across domains and languages. *arXiv preprint arXiv:2506.11350*, 2025.
- Matthijs Douze, Alexandr Guzhva, Chengqi Deng, Jeff Johnson, Gergely Szilvasy, Pierre-Emmanuel Mazaré, Maria Lomeli, Lucas Hosseini, and Hervé Jégou. The faiss library. *IEEE Transactions on Big Data*, 2025.
- Konstantinos Drossos, Samuel Lipping, and Tuomas Virtanen. Clotho: An audio captioning dataset. In *ICASSP 2020-2020 IEEE International Conference on Acoustics, Speech and Signal Processing (ICASSP)*, pages 736–740. IEEE, 2020.
- Paul-Ambroise Duquenne, Holger Schwenk, and Benoît Sagot. Sonar: sentence-level multimodal and language-agnostic representations. *arXiv preprint arXiv:2308.11466*, 2023.
- Debidatta Dwibedi, Yusuf Aytar, Jonathan Tompson, Pierre Sermanet, and Andrew Zisserman. With a little help from my friends: Nearest-neighbor contrastive learning of visual representations. In *Proceedings of the IEEE/CVF international conference on computer vision*, pages 9588–9597, 2021.
- Yuan Gong, Yu-An Chung, and James Glass. Ast: Audio spectrogram transformer. *arXiv preprint arXiv:2104.01778*, 2021.
- Kelvin Guu, Kenton Lee, Zora Tung, Panupong Pasupat, and Mingwei Chang. Retrieval augmented language model pre-training. In *International conference on machine learning*, pages 3929–3938. PMLR, 2020.
- Andrey Guzhov, Federico Raue, Jörn Hees, and Andreas Dengel. Audioclip: Extending clip to image, text and audio. In *ICASSP 2022-2022 IEEE International Conference on Acoustics, Speech and Signal Processing (ICASSP)*, pages 976–980. IEEE, 2022.
- Kaiming He, Haoqi Fan, Yuxin Wu, Saining Xie, and Ross Girshick. Momentum contrast for unsupervised visual representation learning. In *Proceedings of the IEEE/CVF conference on computer vision and pattern recognition*, pages 9729–9738, 2020.
- Roy Rudolf Huizen and Florentina Tatrini Kurniati. Feature extraction with mel scale separation method on noise audio recordings. *arXiv preprint arXiv:2112.14930*, 2021.
- Urvashi Khandelwal, Omer Levy, Dan Jurafsky, Luke Zettlemoyer, and Mike Lewis. Generalization through memorization: Nearest neighbor language models. *arXiv preprint arXiv:1911.00172*, 2019.
- Chris Dongjoo Kim, Byeongchang Kim, Hyunmin Lee, and Gunhee Kim. Audiocaps: Generating captions for audios in the wild. In *Proceedings of the 2019 Conference of the North American Chapter of the Association for Computational Linguistics: Human Language Technologies, Volume 1 (Long and Short Papers)*, pages 119–132, 2019.
- Diederik P Kingma and Jimmy Ba. Adam: A method for stochastic optimization. *arXiv preprint arXiv:1412.6980*, 2014.
- Qiuqiang Kong, Yin Cao, Turab Iqbal, Yuxuan Wang, Wenwu Wang, and Mark D Plumbley. Panns: Large-scale pre-trained audio neural networks for audio pattern recognition. *IEEE/ACM Transactions on Audio, Speech, and Language Processing*, 28:2880–2894, 2020.
- Solomon Kullback and Richard A Leibler. On information and sufficiency. *The annals of mathematical statistics*, 22(1): 79–86, 1951.

- Kuang-Huei Lee, Xi Chen, Gang Hua, Houdong Hu, and Xiaodong He. Stacked cross attention for image-text matching. In *Proceedings of the European conference on computer vision (ECCV)*, pages 201–216, 2018.
- Jiasen Lu, Dhruv Batra, Devi Parikh, and Stefan Lee. ViLbert: Pretraining task-agnostic visiolinguistic representations for vision-and-language tasks. *Advances in neural information processing systems*, 32, 2019.
- Xinhao Mei, Xubo Liu, Jianyuan Sun, Mark Plumbley, and Wenwu Wang. On metric learning for audio-text cross-modal retrieval. In *Proc. Interspeech 2022*, pages 4142–4146, 2022.
- Xinhao Mei, Chutong Meng, Haohe Liu, Qiuqiang Kong, Tom Ko, Chengqi Zhao, Mark D Plumbley, Yuexian Zou, and Wenwu Wang. Wavcaps: A chatgpt-assisted weakly-labelled audio captioning dataset for audio-language multimodal research. *IEEE/ACM Transactions on Audio, Speech, and Language Processing*, 32:3339–3354, 2024.
- Tomas Mikolov, Ilya Sutskever, Kai Chen, Greg S Corrado, and Jeff Dean. Distributed representations of words and phrases and their compositionality. *Advances in neural information processing systems*, 26, 2013.
- Yingqi Qu, Yuchen Ding, Jing Liu, Kai Liu, Ruiyang Ren, Wayne Xin Zhao, Daxiang Dong, Hua Wu, and Haifeng Wang. Rocketqa: An optimized training approach to dense passage retrieval for open-domain question answering. In *Proceedings of the 2021 conference of the North American chapter of the association for computational linguistics: human language technologies*, pages 5835–5847, 2021.
- Alec Radford, Jong Wook Kim, Chris Hallacy, Aditya Ramesh, Gabriel Goh, Sandhini Agarwal, Girish Sastry, Amanda Askell, Pamela Mishkin, Jack Clark, et al. Learning transferable visual models from natural language supervision. In *International conference on machine learning*, pages 8748–8763. PmLR, 2021.
- Bing Su and Gang Hua. Order-preserving wasserstein distance for sequence matching. In *Proceedings of the IEEE conference on computer vision and pattern recognition*, pages 1049–1057, 2017.
- Luoyi Sun, Xuenan Xu, Mengyue Wu, and Weidi Xie. Autoacd: A large-scale dataset for audio-language representation learning. In *Proceedings of the 32nd ACM International Conference on Multimedia*, pages 5025–5034, 2024.
- Ho-Hsiang Wu, Prem Seetharaman, Kundan Kumar, and Juan Pablo Bello. Wav2clip: Learning robust audio representations from clip. In *ICASSP 2022-2022 IEEE International Conference on Acoustics, Speech and Signal Processing (ICASSP)*, pages 4563–4567. IEEE, 2022.
- Yusong Wu, Christos Tsirigotis, Ke Chen, Cheng-Zhi Anna Huang, Aaron Courville, Oriol Nieto, Prem Seetharaman, and Justin Salamon. Flam: Frame-wise language-audio modeling. In *Forty-second International Conference on Machine Learning*.
- Yuxin Xie, Zhihong Zhu, Xianwei Zhuang, Liming Liang, Zhichang Wang, and Yuexian Zou. Gpa: Global and prototype alignment for audio-text retrieval. In *Proc. Interspeech 2024*, pages 5078–5082, 2024.
- Lee Xiong, Chenyan Xiong, Ye Li, Kwok-Fung Tang, Jialin Liu, Paul N Bennett, Junaid Ahmed, and Arnold Overwijk. Approximate nearest neighbor negative contrastive learning for dense text retrieval. In *International Conference on Learning Representations*.
- Xuenan Xu, Zhiling Zhang, Zelin Zhou, Pingyue Zhang, Zeyu Xie, Mengyue Wu, and Kenny Q Zhu. Blat: Bootstrapping language-audio pre-training based on audioset tag-guided synthetic data. In *Proceedings of the 31st ACM International Conference on Multimedia*, pages 2756–2764, 2023.
- Zhiyong Yan, Heinrich Dinkel, Yongqing Wang, Jizhong Liu, Junbo Zhang, Yujun Wang, and Bin Wang. Bridging language gaps in audio-text retrieval. In *Proc. Interspeech 2024*, pages 1675–1679, 2024.
- Yuguo Yin, Yuxin Xie, Wenyuan Yang, Dongchao Yang, Jinghan Ru, Xianwei Zhuang, Liming Liang, and Yuexian Zou. Atri: Mitigating multilingual audio text retrieval inconsistencies by reducing data distribution errors. In *Proceedings of the 63rd Annual Meeting of the Association for Computational Linguistics (Volume 1: Long Papers)*, pages 5491–5504, 2025.
- Tianqi Zhao, Ming Kong, Tian Liang, Qiang Zhu, Kun Kuang, and Fei Wu. Clap: Contrastive language-audio pre-training model for multi-modal sentiment analysis. In *Proceedings of the 2023 ACM international conference on multimedia retrieval*, pages 622–626, 2023.

A Derivation and Visualization of RDM’s Impact

This appendix provides a detailed derivation of the relationship between the Representation Drift Mismatch (RDM) and training stability. The core premise of RDM is that a model’s representation space is non-stationary during training. We first provide a visualization in Figure 6 that empirically demonstrates this phenomenon. It shows how the embeddings of the same audio clips, encoded by a model without dynamic updates, drift significantly as training progresses. Our goal in the following sections is to formally prove that this observed drift leads to a greater potential for gradient misalignment.

Gradient Formulation. We consider a simplified loss function $\mathcal{L} = \mathcal{L}_{\text{main}}(u_i, u'_i)$ that incorporates a knowledge-enhanced representation $u'_i = (1 - \rho)u_i + \rho\mathcal{K}$, where $u_i = f_{\theta_i}(a_i)$ and \mathcal{K} is the expected representation of retrieved knowledge. Formally, $\mathcal{K} = \sum_j P(j)z_j$, where z_j denotes the embedding vector of the j -th sample in the knowledge base, and $P(j)$ is its corresponding probability weight. The gradient of the loss with respect to the model parameters θ_i is:

$$\nabla_{\theta_i} \mathcal{L} = \left(\frac{\partial \mathcal{L}}{\partial u_i} + (1 - \rho) \frac{\partial \mathcal{L}}{\partial u'_i} \right) \frac{\partial u_i}{\partial \theta_i} \quad (22)$$

Linking Gradient Deviation to Knowledge Deviation. The difference between the ideal gradient ($\nabla_{\theta_i} \mathcal{L}_{\text{ideal}}$) and the actual gradient ($\nabla_{\theta_i} \mathcal{L}_{\text{actual}}$) arises from the difference in their respective knowledge vectors, $\mathcal{K}_{\text{ideal}}$ and $\mathcal{K}_{\text{actual}}$. Let the gradient difference vector be $\Delta \nabla = \nabla_{\theta_i} \mathcal{L}_{\text{actual}} - \nabla_{\theta_i} \mathcal{L}_{\text{ideal}}$. This difference is primarily driven by the change in the loss derivative term $\frac{\partial \mathcal{L}}{\partial u_i}$.

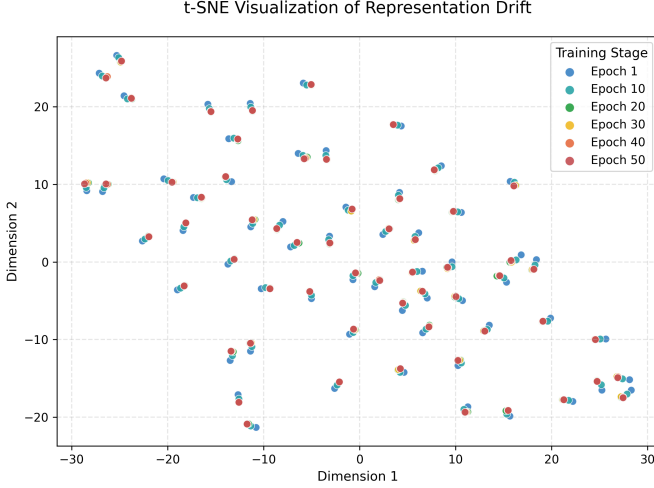


Figure 6: t-SNE visualization of Representation Drift. Embeddings of a fixed set of audio samples, encoded by the same model at different training epochs, are plotted. The progressive shift in embedding positions (from Epoch 1 [blue] to Epoch 50 [red]) empirically validates the core premise of RDM: a static knowledge base becomes misaligned with the non-stationary representation space over time.

To analyze this relationship, we use a first-order Taylor expansion of the loss gradient term around the ideal representation u'_{ideal} . The difference can be approximated as:

$$\frac{\partial \mathcal{L}_{\text{actual}}}{\partial u'_i} - \frac{\partial \mathcal{L}_{\text{ideal}}}{\partial u'_i} \approx H_{\mathcal{L}}(u'_{\text{ideal}}) \cdot (u'_{\text{actual}} - u'_{\text{ideal}}) \quad (23)$$

where $H_{\mathcal{L}}$ is the Hessian matrix of the loss function with respect to its input. Since $u'_{\text{actual}} - u'_{\text{ideal}} = \rho(\mathcal{K}_{\text{actual}} - \mathcal{K}_{\text{ideal}}) = \rho \Delta \mathcal{K}$, we can see that the deviation in the loss gradient is approximately proportional to the deviation in the knowledge vector:

$$\Delta \nabla \propto H_{\mathcal{L}} \cdot \Delta \mathcal{K} \quad (24)$$

This establishes a direct relationship: a larger deviation in the fused knowledge vector $\Delta \mathcal{K}$ leads to a larger deviation in the final parameter gradient $\Delta \nabla$. The next step is therefore to bound the magnitude of $\Delta \mathcal{K}$ using the RDM.

Bounding the Knowledge Deviation via RDM We now bound the norm of the deviation $\|\Delta \mathcal{K}\|_2$ using the RDM. We leverage Pinsker’s inequality, which relates the KL divergence to the Total Variation Distance (D_{TV}):

$$\begin{aligned} D_{TV}(P_1, P_2) &= \frac{1}{2} \sum_j |P_1(j) - P_2(j)| \\ &\leq \sqrt{\frac{1}{2} D_{KL}(P_1 \| P_2)} \end{aligned} \quad (25)$$

Applying this to our distributions gives $D_{TV}(P_{\text{ideal}}, P_{\text{actual}}) \leq \sqrt{\frac{1}{2} \text{RDM}(t, t_k)}$. We can then bound

$\|\Delta \mathcal{K}\|_2$:

$$\begin{aligned} \|\Delta \mathcal{K}\|_2 &= \left\| \sum_j (P_{\text{actual}}(j) - P_{\text{ideal}}(j)) z_j \right\|_2 \\ &\leq \sum_j |P_{\text{actual}}(j) - P_{\text{ideal}}(j)| \|z_j\|_2 \\ &\leq \left(\max_j \|z_j\|_2 \right) \cdot 2 \cdot D_{TV}(P_{\text{ideal}}, P_{\text{actual}}) \\ &\leq C \sqrt{2 \cdot \text{RDM}(t, t_k)} \end{aligned} \quad (26)$$

where $C = \max_j \|z_j\|_2$ is a bounded constant.

Conclusion. Combining these steps, we have established a formal link: an increase in RDM widens the upper bound on the knowledge vector deviation $\|\Delta \mathcal{K}\|_2$ (Eq. 26), which in turn increases the potential magnitude of the gradient deviation $\Delta \nabla$ (Eq. 23). This increases the risk of gradient misalignment, which can lead to training instability. Our dynamic knowledge refinement mechanism is designed to mitigate this risk by periodically resetting the RDM to zero.

B Theoretical Justification and Convergence of the ASK Objective

In this section, we provide a complete theoretical justification for the ASK framework. We demonstrate that our training procedure can be viewed as a principled alternating optimization algorithm designed to maximize the log-likelihood of the observed data, which in turn guarantees the monotonic non-increase of our final loss function and thus ensures convergence.

Probabilistic Formulation with Latent Knowledge. The primary goal of Audio-Text Retrieval is to find model parameters θ^* that maximize the log-likelihood of observing matched audio-text pairs $x_i = (a_i, t_i)$:

$$\theta^* = \max_{\theta} \mathcal{L}(\theta) = \max_{\theta} \sum_i \log p(x_i; \theta) \quad (27)$$

We conceptualize our approach by introducing latent variables, $z_i = (z_{i,f}, z_{i,c})$, representing the unobserved optimal knowledge for each sample x_i . The observed data likelihood is the marginal likelihood over these latent variables:

$$p(x_i; \theta) = \sum_{z_i} p(x_i, z_i; \theta) \quad (28)$$

Thus, the optimization objective becomes:

$$\theta^* = \max_{\theta} \sum_i \log \sum_{z_i} p(x_i, z_i; \theta) \quad (29)$$

The summation inside the logarithm makes direct optimization intractable.

Deriving the Evidence Lower Bound. To create a tractable objective, we introduce an arbitrary distribution $Q(z_i)$ and apply Jensen’s Inequality to derive a lower bound on the log-likelihood, known as the Evidence Lower Bound (ELBO), de-

noted as $\mathcal{F}(Q, \theta)$:

$$\begin{aligned} \log p(x_i; \theta) &= \log \sum_{z_i} Q(z_i) \frac{p(x_i, z_i; \theta)}{Q(z_i)} \\ &\geq \sum_{z_i} Q(z_i) \log \frac{p(x_i, z_i; \theta)}{Q(z_i)} \end{aligned} \quad (30)$$

$$\begin{aligned} \mathcal{F}(Q, \theta) &= \mathbb{E}_{Q(z_i)}[\log p(x_i, z_i; \theta)] \\ &\quad - \mathbb{E}_{Q(z_i)}[\log Q(z_i)] \end{aligned} \quad (31)$$

Maximizing $\log p(x_i; \theta)$ is achieved by iteratively maximizing this lower bound \mathcal{F} with respect to Q and θ .

The ASK Framework as an Alternating Optimization Algorithm. Let θ_t be the parameters at iteration t . The ASK training process alternates between two stages.

Stage 1: Auxiliary Distribution Update. In this stage, we fix θ_t and approximate the optimal auxiliary distribution $Q_t(z_i)$ which should be the true posterior $p(z_i|x_i; \theta_t)$. We assume independence between fine- and coarse-grained knowledge: $Q_t(z_i) = Q_{t,f}(z_{i,f})Q_{t,c}(z_{i,c})$.

- The retrieval of Top-K neighbors defines the support of $Q_{t,f}$ and $Q_{t,c}$.
- We define the probability mass of these distributions over a specific neighbor z_j using our reliability weights:

$$\begin{aligned} Q_{t,f}(z_{i,f} = z_j) &:= w_{j,f}(\theta_t), \\ Q_{t,c}(z_{i,c} = z_j) &:= w_{j,c}(\theta_t) \end{aligned} \quad (32)$$

Stage 2: Model Parameter Update. In this stage, we fix Q_t and maximize the ELBO with respect to θ , which is equivalent to maximizing $\mathbb{E}_{Q_t}[\log p(x_i, z_i; \theta)]$. We model the joint log-probability as a sum of independent fine- and coarse-grained components, e.g., for the text-to-audio direction:

$$\begin{aligned} \log p(x_i, z_i; \theta) &\approx \left(-\mathcal{L}_{OT,f}(\theta) - \log \Psi_{i,f}^{T \leftarrow A}(\theta) \right) \\ &\quad + \left(-\mathcal{L}_{OT,c}(\theta) - \log \Psi_{i,c}^{T \leftarrow A}(\theta) \right) \\ &\quad + (-\log Z(\theta)) \end{aligned} \quad (33)$$

where $Z(\theta)$ is a normalization constant. The maximization objective is to minimize the negative expectation of this log-probability under Q_t . Substituting Eq. 32 and Eq. 33, this objective becomes:

$$\begin{aligned} \mathcal{L}_m &= - \sum_i \mathbb{E}_{Q_t(z_i)}[\log p(x_i, z_i; \theta)] \\ &\approx \sum_i (\mathbb{E}_{Q_{t,f}}[\mathcal{L}_{OT,f} + \log \Psi_{i,f}] \\ &\quad + \mathbb{E}_{Q_{t,c}}[\mathcal{L}_{OT,c} + \log \Psi_{i,c}]) \end{aligned} \quad (34)$$

Our final modulated loss,

$$\mathcal{L}_{T \rightarrow A}^* = (1 + \lambda_f \mathcal{F}_f^{T \rightarrow A} + \lambda_c \mathcal{F}_c^{T \rightarrow A}) \cdot \mathcal{L}_{T \rightarrow A} \quad (35)$$

where $\mathcal{F} = -\log \Psi$, is a principled and sophisticated implementation of this maximization objective. Minimizing \mathcal{L}_{ASK} effectively performs this parameter update.

Proof of Convergence. This two-stage alternating optimization guarantees that the total objective is non-decreasing at each full iteration, $\mathcal{L}(\theta_{t+1}) \geq \mathcal{L}(\theta_t)$. Consequently, minimizing the negative log-likelihood guarantees that the loss is monotonically non-increasing. Given that \mathcal{L}_{ASK} is bounded below by zero, the Monotone Convergence Theorem ensures that the sequence of loss values converges to a limit, and the parameters $\{\theta_t\}$ converge to a stationary point

C Optimal Transport for Batch-level Alignment

This section details the entropy-regularized Optimal Transport (OT) formulation used to refine the batch-wise similarity matrices. Given a batch of knowledge-enhanced pairs, we compute a similarity matrix, e.g., the fine-grained matrix $\mathbf{S}_f \in \mathbb{R}^{B \times B}$. We then seek an optimal transport plan $\mathbf{Q} \in \mathbb{R}^{B \times B}$, where \mathbf{Q}_{ij} represents the soft-alignment probability between the i -th text and the j -th audio. The optimal plan \mathbf{Q}^* is found by solving the following regularized optimization problem:

$$\mathbf{Q}^* = \max_{\mathbf{Q} \in C} \langle \mathbf{Q}, \mathbf{S}_f \rangle + \varepsilon H(\mathbf{Q}) \quad (36)$$

$$\text{s.t. } C = \{ \mathbf{Q} \in \mathbb{R}^{B \times B} \mid \mathbf{Q} \mathbf{1}_B = \boldsymbol{\mu}, \mathbf{Q}^\top \mathbf{1}_B = \boldsymbol{\nu} \},$$

where $\langle \mathbf{Q}, \mathbf{S}_f \rangle = \text{tr}(\mathbf{Q}^\top \mathbf{S}_f)$ is the total similarity score. $H(\mathbf{Q}) = -\sum_{i,j} \mathbf{Q}_{ij} \log \mathbf{Q}_{ij}$ is the entropy regularizer, controlled by $\varepsilon > 0$. The constraints enforce that the marginals of \mathbf{Q} must sum to predefined distributions $\boldsymbol{\mu}$ and $\boldsymbol{\nu}$, which represent the importance of each instance. Following prior work [Su and Hua, 2017], we set both $\boldsymbol{\mu}$ and $\boldsymbol{\nu}$ to a uniform distribution over the batch, i.e., $\frac{1}{|B|} \mathbf{1}_{|B|}$. This problem is efficiently solved for the optimal plan \mathbf{Q}^* using the Sinkhorn-Knopp algorithm [Cuturi, 2013].

D Full Results for Local Interaction Strategy

This section provides the complete retrieval results for our experiments on the local, token-level interaction baselines, including both Audio-to-Text and Text-to-Audio directions. Table 4 presents the full comparison against both the FLAM and GPA architectures.

As demonstrated in Table 4, ASK consistently outpaces both baselines across all metrics in the Text-to-Audio retrieval direction as well. When compared to the stronger GPA baseline, ASK⁺ achieves the highest R@1 score on AudioCaps, yielding a 1.0% absolute improvement, which translates to a substantial 2.0% margin over FLAM. On Clotho, the ASK^{*} variant delivers the strongest R@1 performance with a significant gain of 1.2% absolute over GPA, and a notable 2.5% absolute advantage over FLAM. These results confirm that the benefits of our proposed mechanisms are symmetric, enhancing both retrieval directions and validating the overall effectiveness of the ASK framework on fine-grained architectures.

E Comparison with Alternative Retrieval-Augmented Frameworks

To further validate the design choices of our ASK framework, we compare it against classical retrieval-augmented contrastive learning paradigms adapted from computer vision and information retrieval. Specifically, we benchmark against representative retrieval-augmented and contrastive learning paradigms:

Table 4: Full results for Audio-Text Retrieval on AudioCaps and Clotho under the local interaction strategy. The symbols ⁺, [†], and * denote different knowledge sources.

Audio-to-Text						
Method	AudioCaps			Clotho		
	R@1	R@5	R@10	R@1	R@5	R@10
FLAM Wu et al.	40.3 _{±0.1}	71.2 _{±0.3}	83.6 _{±0.2}	17.5 _{±0.1}	38.8 _{±0.4}	50.5 _{±0.4}
GPA Xie et al. [2024]	41.1 _{±0.3}	73.8 _{±0.4}	85.2 _{±0.6}	18.1 _{±0.2}	40.2 _{±0.3}	53.4 _{±0.4}
ASK [†]	42.9 _{±0.3}	75.1 _{±0.6}	86.4 _{±0.5}	19.1 _{±0.1}	41.9 _{±0.4}	53.9 _{±0.8}
ASK*	43.7 _{±0.2}	75.8 _{±0.3}	86.2 _{±0.7}	19.2 _{±0.3}	41.6 _{±0.7}	54.5 _{±0.6}
ASK ⁺	43.1 _{±0.3}	74.0 _{±0.6}	86.9 _{±0.5}	19.5 _{±0.3}	41.4 _{±0.7}	54.5 _{±0.6}
Text-to-Audio						
Method	AudioCaps			Clotho		
	R@1	R@5	R@10	R@1	R@5	R@10
FLAM Wu et al.	33.1 _{±0.1}	67.5 _{±0.2}	80.0 _{±0.2}	13.8 _{±0.2}	33.2 _{±0.3}	45.1 _{±0.2}
GPA Xie et al. [2024]	34.1 _{±0.2}	70.0 _{±0.4}	82.2 _{±0.6}	15.1 _{±0.2}	37.9 _{±0.6}	50.2 _{±0.4}
ASK [†]	34.5 _{±0.3}	71.1 _{±0.6}	83.1 _{±0.6}	16.2 _{±0.1}	38.5 _{±0.4}	51.3 _{±0.5}
ASK*	34.6 _{±0.2}	70.5 _{±0.5}	82.7 _{±0.6}	16.3 _{±0.2}	38.4 _{±0.3}	51.5 _{±0.4}
ASK ⁺	35.1 _{±0.3}	70.8 _{±0.5}	83.1 _{±0.4}	16.0 _{±0.1}	38.8 _{±0.3}	52.1 _{±0.5}

MoCo He et al. [2020], ANCE Xiong et al., and NNCLR Dwibedi et al. [2021]. These baselines represent the classical strategies for expanding negative sample capacity, performing hard negative mining, and utilizing external support sets, respectively. We adapt their core mechanisms to the Audio-Text Retrieval setting. All variants are built upon the identical ML-ACT Mei et al. [2022] backbone to ensure a fair and rigorous comparison.

Table 5: Comparison with other retrieval-augmented methods on AudioCaps. The symbol + denotes using training set as the knowledge source

Method	Audio-to-Text			Text-to-Audio		
	R@1	R@5	R@10	R@1	R@5	R@10
ML-ACT Mei et al. [2022]	36.3 _{±0.5}	68.6 _{±0.3}	81.5 _{±0.2}	32.2 _{±0.4}	68.2 _{±0.1}	81.2 _{±0.2}
NNCLR Dwibedi et al. [2021]	32.5 _{±0.9}	66.6 _{±0.5}	80.9 _{±0.7}	30.2 _{±0.3}	64.9 _{±0.1}	80.1 _{±0.1}
ANCE Xiong et al.	35.9 _{±0.5}	67.8 _{±0.3}	83.6 _{±0.2}	31.7 _{±0.1}	65.4 _{±0.5}	79.8 _{±0.1}
MoCo He et al. [2020]	37.2 _{±0.3}	68.5 _{±0.5}	82.0 _{±0.3}	32.9 _{±0.4}	67.4 _{±0.6}	80.9 _{±0.1}
ASK ⁺	42.0 _{±0.2}	74.2 _{±0.5}	85.4 _{±0.6}	35.4 _{±0.3}	70.2 _{±0.3}	83.1 _{±0.7}

As shown in Table 5, our proposed ASK significantly outperforms all alternative strategies across all metrics, achieving an R@1 of 42.0% in Audio-to-Text retrieval. Conversely, directly migrating classical contrastive methods to the Audio-Text Retrieval (ATR) domain yields sub-optimal or degraded performance. While MoCo provides only marginal improvements, both ANCE and NNCLR lead to noticeable performance drops, with NNCLR causing the most severe degradation (e.g., Audio-Text R@1 dropping from 36.3% to 32.5%).

We hypothesize that this performance degradation stems from the unique semantic ambiguities in ATR. Specifically, methods relying on strict hard negative mining (ANCE) or unimodal nearest neighbors (NNCLR) are highly susceptible to acoustic confusion, which inadvertently introduces false negatives or modality-specific noise into the contrastive objective. Additionally, the memory queues in MoCo may suffer from representation drift due to the continuous updating of the fine-grained

audio encoder. Unlike these rigid mechanisms, ASK mitigates these domain-specific bottlenecks by employing an adaptive reliability weighting scheme that explicitly evaluates cross-modal consistency, effectively filtering out the retrieval noise that limits standard baselines.

F Hyperparameter Sensitivity Analysis

To comprehensively evaluate the robustness of the proposed ASK framework, we conduct sensitivity analyses on two critical hyperparameters: the retrieved knowledge size (K) and the knowledge injection ratio (ρ). The experiments are conducted on the AudioCaps dataset using the ASK⁺ variant. The results are illustrated in Figure 7.

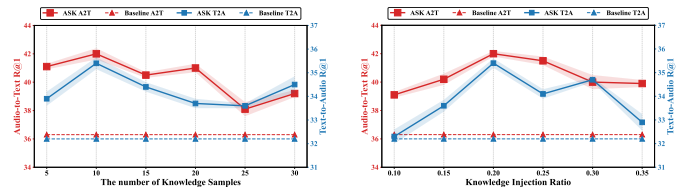


Figure 7: Hyperparameter sensitivity analysis. Left: Impact of the retrieved knowledge size K . Right: Impact of the knowledge injection ratio ρ .

Impact of the Retrieved Knowledge Size (K). The left panel of Figure 7 illustrates the effect of varying the number of retrieved knowledge samples K from 5 to 30. The framework achieves its optimal performance in both Audio-to-Text (A2T) and Text-to-Audio (T2A) retrieval at $K = 10$, reaching a peak A2T R@1 of 42.0% and T2A R@1 of 35.4%. When K is set too small (e.g., $K = 5$), the limited neighborhood fails to provide sufficient semantic diversity, restricting the model’s ability to generalize to ambiguous or long-tail concepts. Conversely, setting K too large (e.g., $K \geq 15$) inevitably introduces acoustically similar but semantically irrelevant noise into the knowledge base. This excessive retrieval dilutes the valid semantic guidance and consequently degrades the alignment performance.

Impact of the Knowledge Injection Ratio (ρ). The right panel of Figure 7 presents the performance fluctuations across different knowledge injection ratios $\rho \in [0.10, 0.35]$. This hyperparameter controls the crucial trade-off between retaining the original instance identity and incorporating the retrieved global semantic prior. As shown in the figure, the model attains its peak performance at $\rho = 0.20$. A lower injection ratio (e.g., $\rho = 0.10$) provides insufficient global context, making it difficult to fully break the Gradient Locality Bottleneck (GLB). However, an excessively high ratio ($\rho \geq 0.25$) over-dominates the feature fusion process. This leads to feature homogenization, where the unique acoustic or textual characteristics of the original sample are overshadowed by the aggregated neighborhood representations, ultimately resulting in a decline in retrieval accuracy.

G Visualization of Adaptive Reliability Weighting

To explicitly address how the Adaptive Reliability Weighting mechanism mitigates Representation-Drift Mismatch (RDM)

and filters noise, we delve into the mathematical behavior of the reliability potential $\mathcal{F} = -\log \Psi$. We provide an internal visualization of these assigned weights during the training process to demonstrate their dynamic modulation effects.

A critical but nuanced property of our framework is that \mathcal{F} acts as a dynamic negative regularizer. Given the normalized embedding space, the cross-modal similarity generally maintains non-negative exponential characteristics, leading to an expected similarity $\Psi \geq 1$. Consequently, the reliability weight \mathcal{F} consistently operates in the negative domain ($\mathcal{F} \leq 0$). This design intrinsically serves as a reward mechanism that dynamically relaxes the standard in-batch contrastive penalty when reliable external knowledge is injected.

Table 6 illustrates this internal mechanism using two challenging acoustic ambiguity scenarios. Query 1 involves confusing environmental textures (“*Thunder*” vs. “*Sizzling food*”). Query 2, drawn directly from our evaluation set, involves engine and wind noises where a “*Motorboat*” could be acoustically confused with a “*Motorcycle*”.

Table 6: Internal visualization of the reliability potential Ψ and the negative regularizer weight \mathcal{F} .

Neighborhood State	Semantic Concept	Ψ	\mathcal{F}	Modulation
Query 1: “Thunder roars in the distance as rain falls” (Environmental Texture Ambiguity)				
Clean Neighborhood	“Loud thunder claps”	1.60	-0.47	0.91
Noise Neighborhood	“Food sizzling loudly”	1.05	-0.05	0.99
Query 2: “A motorboat driving by as water splashes and wind blows” (Vehicle Engine Ambiguity)				
Clean Neighborhood	“A speedboat traveling across water”	1.55	-0.44	0.91
Noise Neighborhood	“A motorcycle engine revving”	1.08	-0.08	0.98

When the retrieved neighborhood contains highly relevant concepts (e.g., “*Loud thunder claps*” or “*A speedboat traveling*”), the strong semantic alignment yields a larger $\Psi (> 1)$, forcing \mathcal{F} to be a distinctively negative value with a large magnitude (e.g., -0.47 and -0.44). This dynamically reduces the modulation multiplier $(1 + \lambda\mathcal{F}) < 1$, effectively rewarding the model by down-weighting the standard contrastive penalty and encouraging the absorption of this clean knowledge.

Conversely, when the retrieved knowledge is corrupted by RDM drift—such as retrieving the acoustically similar but semantically incorrect “*Food sizzling loudly*” or “*A motorcycle engine revving*”—the weak cross-modal alignment results in a Ψ closer to 1. This causes the negative regularizer \mathcal{F} to approach zero (e.g., -0.05 and -0.08), which pulls the modulation multiplier back to near 1.0. By doing so, the framework withholds the reward and maintains the strict original contrastive loss, seamlessly preventing the model from over-relying on the drifted acoustic noise.